

# The Heme Environment of Recombinant Human Indoleamine 2,3-Dioxygenase

STRUCTURAL PROPERTIES AND SUBSTRATE-LIGAND INTERACTIONS\*

Received for publication, January 15, 2002, and in revised form, February 9, 2002  
Published, JBC Papers in Press, February 26, 2002, DOI 10.1074/jbc.M200457200

Andrew C. Terentis‡, Shane R. Thomas‡, Osamu Takikawa§, Tamantha K. Littlejohn¶, Roger J. W. Truscott¶, Robert S. Armstrong||, Syun-Ru Yeh\*\*, and Roland Stocker‡ ‡‡

From the ‡Biochemistry Group, The Heart Research Institute, 145 Missenden Road, Camperdown, New South Wales 2050, Australia, the §Department of Pharmacology, Hokkaido University, Sapporo 060-8638, Japan, the ¶Australian Cataract Research Foundation, University of Wollongong, Wollongong, New South Wales 2522, Australia, the ||School of Chemistry, The University of Sydney, Sydney, New South Wales 2006, Australia, and the \*\*Department of Physiology and Biophysics, Albert Einstein College of Medicine, Bronx, New York 10461

Indoleamine 2,3-dioxygenase is a heme enzyme that catalyzes the oxidative degradation of L-Trp and other indoleamines. We have used resonance Raman spectroscopy to characterize the heme environment of purified recombinant human indoleamine 2,3-dioxygenase (hIDO). In the absence of L-Trp, the spectrum of the Fe<sup>3+</sup> form displayed six-coordinate, mixed high and low spin character. Addition of L-Trp triggered a transition to predominantly low spin with two Fe-OH<sup>-</sup> stretching modes identified at 546 and 496 cm<sup>-1</sup>, suggesting H-bonding between the NH group of the pyrrole ring of L-Trp and heme-bound OH<sup>-</sup>. The distal pocket of Fe<sup>3+</sup> hIDO was explored further by an exogenous heme ligand, CN<sup>-</sup>; again, binding of L-Trp introduced strong H-bonding and/or steric interactions to the heme-bound CN<sup>-</sup>. On the other hand, the spectrum of Fe<sup>2+</sup> hIDO revealed a five-coordinate and high spin heme with or without L-Trp bound. The proximal Fe-His stretching mode, identified at 236 cm<sup>-1</sup>, did not shift upon L-Trp addition, indicating that the proximal Fe-His bond strength is not affected by binding of the substrate. The high Fe-His stretching frequency suggests that Fe<sup>2+</sup> hIDO has a strong “peroxidase-like” Fe-His bond. Using CO as a structural probe for the distal environment of Fe<sup>2+</sup> hIDO revealed that binding of L-Trp in the distal pocket converted IDO to a peroxidase-like enzyme. Binding of L-Trp also caused conformational changes to the heme vinyl groups, which were independent of changes of the spin and coordination state of the heme iron. Together these data indicate that the strong proximal Fe-His bond and the strong H-bonding and/or steric interactions between L-Trp and dioxygen in the distal pocket are likely crucial for the enzymatic activity of hIDO.

Indoleamine 2,3-dioxygenase (IDO)<sup>1</sup> catalyzes the cleavage

\* This work was supported by grants from the Australian National Health and Medical Research Council (to R. S.) and by National Institutes of Health Grant HL65465 (to S.-R. Y.). The costs of publication of this article were defrayed in part by the payment of page charges. This article must therefore be hereby marked “advertisement” in accordance with 18 U.S.C. Section 1734 solely to indicate this fact.

‡‡ To whom correspondence should be addressed: Centre for Thrombosis and Vascular Biology, The University of New South Wales, UNSW Sydney 2052, New South Wales, Australia. E-mail: r.stocker@unsw.edu.au.

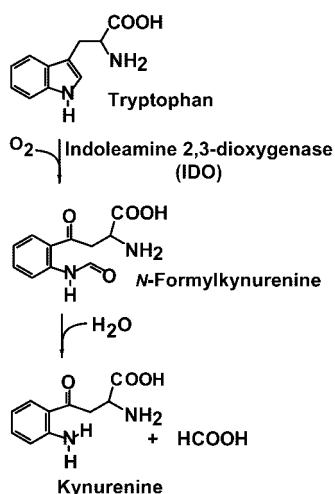
<sup>1</sup> The abbreviations used are: IDO, indoleamine 2,3-dioxygenase; hIDO, recombinant human IDO; rIDO, rabbit intestinal IDO.

of the pyrrole ring of L-Trp and other indoleamines by insertion of molecular oxygen (1, 2). In the case of L-Trp, N-formylkynurenine is the primary product (Scheme 1), and the reaction represents the first and rate-limiting step of the kynurenine pathway, the major Trp catabolic pathway in mammals. The dioxygenase is ubiquitous in nonhepatic tissue where it is induced mainly by interferon- $\gamma$  in response to a variety of infectious agents (such as influenza, tuberculosis, and malaria) and chronic inflammatory disorders (3). The precise role of IDO remains unclear, although its induction and the metabolism of L-Trp along the kynurenine pathway are implicated in a variety of physiological and pathophysiological processes, including antimicrobial and antitumor defense, neuropathology, immunoregulation, and antioxidant activity (3).

IDO is a ~42-kDa monomeric protein containing protoporphyrin IX as the sole prosthetic group that is essential for enzymatic activity (1, 4). Phylogenetic analysis reveals 25–35% amino acid identity with myoglobins (Mbs) of archaeogastropod molluscs (5, 6), suggesting a common ancestral gene. These myoglobins and IDO contain two highly conserved His residues, postulated to be the proximal and distal heme-coordinating residues (6, 7).

To date almost all studies on the purified enzyme have been carried out with rabbit indoleamine 2,3-dioxygenase (rIDO). Indeed the dioxygenase was first isolated from rabbit intestine (1), and the enzyme is invariably purified with the heme iron in the Fe<sup>3+</sup> state. The reduced, catalytically active Fe<sup>2+</sup> form readily autoxidizes, especially in the presence of a substrate (4, 8–10). A reducing cofactor is required to initiate and sustain enzyme activity, and this is usually achieved *in vitro* using methylene blue and ascorbic acid (8, 11, 12). The *in vivo* cofactor(s) remains unknown, with superoxide anion radical being one possible candidate as it can activate rIDO and is incorporated into L-Trp (4, 8–10).

rIDO can bind a variety of relatively large substrates and inhibitors, indicating a large substrate binding pocket (13–16). Previous studies of rIDO using (magnetic) circular dichroism, electronic absorption, and electron paramagnetic resonance (EPR) spectroscopy showed that substrate-free Fe<sup>3+</sup> rIDO is six-coordinate and predominantly high spin and that substrate binding triggers protein conformational changes and an increase in low spin signals due to the coordination of the distal His residue to the heme (17). L-Trp has a higher affinity for Fe<sup>2+</sup> than Fe<sup>2+</sup>-CO and Fe<sup>3+</sup> rIDO, and based on this it was proposed that the Fe<sup>2+</sup> enzyme binds L-Trp before dioxygen in the catalytic reaction cycle (11).



**SCHEME 1. IDO-induced Trp catabolism.** IDO is the first and rate-limiting enzyme in the catabolism of Trp in nonhepatic tissue, incorporating molecular oxygen into the pyrrole ring to yield *N*-formylkynurenine as the primary product. *N*-Formylkynurenine degrades to kynurenine and formic acid.

To investigate the structural features underlying the chemical reactivity of IDO in more detail, we have measured the resonance Raman spectra of recombinant human indoleamine 2,3-dioxygenase (hIDO) and its cyanide, carbon monoxide, and L-Trp complexes. The data show that the distal and proximal heme environments of hIDO are distinctly different from that of conventional Mb and that L-Trp binds closely but not directly to the distal side of the heme iron. Together they suggest that the strong proximal Fe–His bond and the strong H-bonding and/or steric interactions imposed by L-Trp on dioxygen in the distal pocket are likely to play crucial roles in the catalytic reaction of hIDO.

#### EXPERIMENTAL PROCEDURES

**Materials**—CO,  $^{13}\text{C}^{18}\text{O}$ ,  $\text{K}^{13}\text{C}^{15}\text{N}$ ,  $\text{K}^{13}\text{CN}$ , and  $\text{D}_2^{18}\text{O}$  were purchased from Icon (Mt. Marion, NY), and  $\text{KC}^{15}\text{N}$  was from Cambridge Isotopes. All other materials were purchased from Sigma and were of the highest available purity.

**Expression and Purification of hIDO**—hIDO was expressed and purified as a fusion protein to a hexahistidyl tag as detailed elsewhere (18). Previous studies established that the hexahistidyl tag does not affect the physical properties of the enzyme (18). Before use, hIDO was gel-filtered through a Sephadex G-25 column eluted with 100 mM phosphate buffer (pH 7.4) containing 100  $\mu\text{M}$  EDTA. The heme content of hIDO, assessed by the ratio of absorbance at 406 to 280 nm, was  $1.6 \pm 0.2$ , and the specific activity, measured by the methylene blue/ascorbate assay (11), was  $90 \pm 20$  mol of L-Trp/min/mol of enzyme. This activity is comparable to that of native human (89 mol/min/mol; Ref. 18) and rabbit IDO ( $\sim 108$  mol/min/mol; Ref. 11). Measurement of hIDO activity after resonance Raman experiments showed  $<10\%$  loss of activity due to laser-induced damage to the protein.

**Preparation of Sample Complexes**—Concentrated hIDO was diluted to a final concentration of  $\sim 30$   $\mu\text{M}$  in phosphate buffer, and  $\sim 100$   $\mu\text{l}$  was used for resonance Raman measurements in a septum-sealed cell. Ferric and  $\text{Fe}^{2+}\text{-CO}$  hIDO were prepared by anaerobic reduction with sodium dithionite and introduction of CO gas by syringe injection. Ferric cyanide complexes were prepared by addition of a small amount of solid potassium cyanide ( $\text{CN}^-$ ) to the  $\text{Fe}^{3+}$  sample. Stocks of L-Trp (50 mM) were prepared in phosphate buffer and added to samples as indicated. Spectra recorded in  $\text{D}_2^{18}\text{O}$  were prepared by dilution of concentrated hIDO in an appropriate volume of  $\text{D}_2^{18}\text{O}$  (80–90% final volume of  $\text{D}_2^{18}\text{O}$ ). The electronic absorption spectrum of the samples was recorded before and after every experiment to confirm sample purity and stability.

**Resonance Raman Spectroscopy**—All resonance Raman measurements were made using the instrumentation described previously (19). Briefly, the output at 413.1 nm from a krypton ion laser (Spectra Physics, Mountain View, CA) ( $\sim 5$  milliwatts) was focused to a  $\sim 30$ - $\mu\text{m}$  spot on a cell rotating at  $\sim 1000$  rpm. For  $\text{Fe}^{2+}\text{-CO}$  complexes, laser

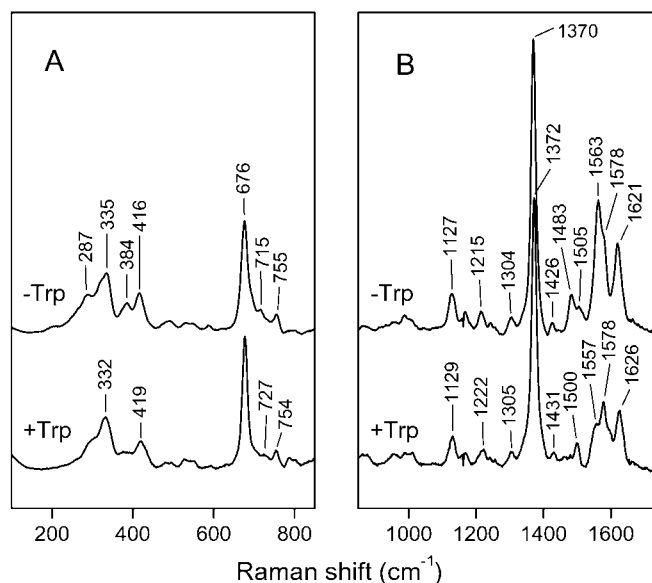


**FIG. 1. Resonance Raman spectra of ferric hIDO in the absence and presence of L-Trp.** Panel A, low frequency region. Panel B, high frequency region. Spectra were obtained using a laser wavelength of 413.1 nm and power of  $\sim 5$  milliwatts in the presence (+Trp, bottom) or absence of L-Trp (–Trp, top) at room temperature and pH 7.4 as described under “Experimental Procedures.” The final concentration of L-Trp was 40 mM.

power was kept at  $<2$  milliwatts to avoid ligand photodissociation. The acquisition time was typically 10–15 min. The scattered light was collected at right angles to the incident beam and focused on the entrance slit (100  $\mu\text{m}$ ) of a 1.25 m Spex spectrometer (Jobin Yvon, Edison, NJ) where it was dispersed and then detected by a CCD camera (Roper Scientific, Princeton, NJ). For calibration, the lines of indene in the 170–1750  $\text{cm}^{-1}$  region were recorded daily. All measurements were done at room temperature.

#### RESULTS

**Ferric hIDO**—We used 413.1 nm laser light in resonance with the strong Soret electronic transition of heme. This yielded a resonance Raman spectrum of  $\text{Fe}^{3+}$  hIDO with several intense bands that can be assigned to totally symmetric vibrational modes of the porphyrin ring system (Fig. 1). For the substrate-free enzyme (Fig. 1B, top), the strongest band was the oxidation-state marker band  $\nu_4$  at 1370  $\text{cm}^{-1}$ , typical for  $\text{Fe}^{3+}$  heme. The high frequency region also showed a heme peripheral vinyl group stretching band at 1621  $\text{cm}^{-1}$ . The porphyrin core-size marker bands  $\nu_3$  and  $\nu_2$  were observed at 1483 and 1563  $\text{cm}^{-1}$ , respectively, characteristic of a six-coordinate high spin heme with shoulders at 1505 and  $\sim 1578$   $\text{cm}^{-1}$ , respectively, characteristic of a six-coordinate low spin heme (20, 21). The mixed spin character of  $\text{Fe}^{3+}$  hIDO is similar to mammalian globins (22) in which the distal side of the heme iron is coordinated by a solvent water molecule.

In the low frequency region of the substrate-free enzyme (Fig. 1A, top), the most intense band was the characteristic heme marker band  $\nu_7$  at 676  $\text{cm}^{-1}$ . The 250–450  $\text{cm}^{-1}$  region of heme proteins displayed several bands that are assigned to porphyrin out-of-plane vibrations, Fe-porphyrin stretching, and peripheral vinyl and propionate group in-plane bending vibrations (23). For hIDO the bands in this region were not resolved well and displayed differences in frequencies and relative intensities compared with sperm whale Mb (23). Nevertheless, using this comparison the intense 335  $\text{cm}^{-1}$  band was assigned to the Fe-porphyrin nitrogen stretching mode  $\nu_8$  with vinyl bending character. The 384 and 416  $\text{cm}^{-1}$  bands were assigned to propionate and vinyl in-plane bending modes, respectively, the frequency and intensity of which are sensitive to

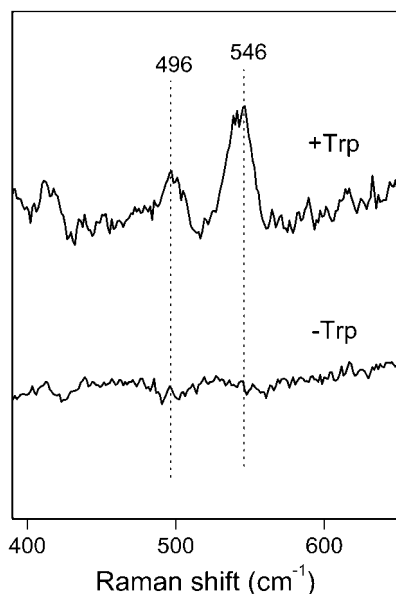


FIG. 2.  $\text{H}_2\text{O}-\text{D}_2^{18}\text{O}$  difference spectra for ferric hIDO in the absence and presence of L-Trp. Experimental conditions were as described in Fig. 1 legend and under "Experimental Procedures." Spectra in  $\text{H}_2\text{O}$  and  $\text{D}_2^{18}\text{O}$  (90%, v/v) were recorded consecutively. The final concentration of L-Trp was 4.5 mM.

conformational changes of these heme peripheral groups (24).

Addition of L-Trp to  $\text{Fe}^{3+}$  hIDO triggered a pronounced transition of the heme iron to six-coordinate and low spin as indicated by the increased intensities of  $\nu_3$  and  $\nu_2$  at 1500 and 1578  $\text{cm}^{-1}$  (Fig. 1B, bottom). To identify the distal ligand of the  $\text{Fe}^{3+}$ -Trp complex, the  $\text{H}_2\text{O}-\text{D}_2^{18}\text{O}$  difference spectrum was obtained. In the isotope difference spectrum, all the heme modes are canceled out except those associated with the heme-bound hydroxide or water. Two vibrational bands at 546 and 496  $\text{cm}^{-1}$  were observed (Fig. 2). They are similar to the  $\sim 550$  and  $\sim 490$   $\text{cm}^{-1}$  bands observed in the alkaline form of globins (Table I), which were assigned to the  $\text{Fe}-\text{OH}^-$  stretching modes ( $\nu_{\text{Fe}-\text{OH}^-}$ ) of the low spin and high spin heme, respectively (19, 22). Similarly we assigned the two bands in the hIDO  $\text{Fe}^{3+}$ -Trp difference spectrum to  $\nu_{\text{Fe}-\text{OH}^-}$ , although both bands may correspond to the same low spin species as a high spin species was not seen in the high frequency region of the spectrum (Fig. 1B, bottom). In the absence of L-Trp  $\nu_{\text{Fe}-\text{OH}^-}$  bands were not observed for  $\text{Fe}^{3+}$  hIDO (Fig. 2) even at pH 10 when the distal water molecule was partially deprotonated and the contribution from the six-coordinate low spin component was increased (data not shown). These data suggest that L-Trp binds closely but not directly to the distal side of the heme iron, and the heme-bound hydroxide interacts with the NH group of the pyrrole ring of the L-Trp through an H-bond (Scheme 2, II), which somehow enhances the  $\nu_{\text{Fe}-\text{OH}^-}$  modes. Binding of L-Trp to hIDO also perturbed the heme vinyl groups as shown by the up-shift of the vinyl stretching mode from 1621 to 1626  $\text{cm}^{-1}$  (Fig. 1B) and the vinyl bending mode from 416 to 419  $\text{cm}^{-1}$  (Fig. 1A).

**Ferrous hIDO**—The spectrum of  $\text{Fe}^{2+}$  hIDO provides structural information on the catalytically active enzyme. In the high frequency region, the  $\nu_4$  band appeared intensely at 1353  $\text{cm}^{-1}$  and the  $\nu_3$  band at 1469  $\text{cm}^{-1}$  (Fig. 3B), characteristic of a five-coordinate and high spin  $\text{Fe}^{2+}$  heme with His as a proximal ligand. In the low frequency region, a band at 236  $\text{cm}^{-1}$  (Fig. 3A, top) was assigned as the proximal iron-His stretching mode  $\nu_{\text{Fe}-\text{His}}$ . This frequency is significantly higher than that observed for globins ( $\sim 220$   $\text{cm}^{-1}$ ), although it occurred in the 230–245  $\text{cm}^{-1}$  range commonly observed for peroxidases (21,

25, 26) (Table I). In contrast to the  $\text{Fe}^{3+}$  form, addition of L-Trp did not induce a spin state change to  $\text{Fe}^{2+}$  hIDO as the  $\nu_3$  band remained characteristic of five-coordinate and high spin heme (Fig. 3B, bottom), supporting the notion that the substrate does not bind directly to the heme iron. In addition, the  $\nu_{\text{Fe}-\text{His}}$  (Fig. 3A) remained the same at 236  $\text{cm}^{-1}$ , indicating that the substrate does not affect the strength of the proximal Fe–His bond. The data suggest that the distal coordination position remains free in the catalytically active hIDO, allowing for the binding of dioxygen during the catalytic reaction cycle.

**Cyanide-bound Complex**—It was not possible to study the interaction of  $\text{O}_2$  and L-Trp using the present techniques as the  $\text{O}_2$  complexes were too unstable. Instead we studied the resonance Raman spectra of the  $\text{CN}^-$  and CO complexes of  $\text{Fe}^{3+}$  and  $\text{Fe}^{2+}$  hIDO, respectively, to obtain information on the interactions between the substrate and distal ligands. The high frequency region for the  $\text{CN}^-$  complex displayed characteristics of a six-coordinate, low spin complex (Fig. 4). Addition of L-Trp caused pronounced changes to vinyl-associated bands, such as an increased frequency and intensity of the stretch at 1630  $\text{cm}^{-1}$  (Fig. 4B, bottom), an up-shift and sharpening of the bend at 422  $\text{cm}^{-1}$ , and sharpening of  $\nu_8$  at 328  $\text{cm}^{-1}$  (Fig. 4A). The shoulder at 1639  $\text{cm}^{-1}$  (Fig. 4B, top) was assigned to the porphyrin band  $\nu_{10}$ , which was buried in the strongly enhanced 1630  $\text{cm}^{-1}$  band in the presence of L-Trp.

To further obtain the structural information of the heme bound  $\text{CN}^-$  and thereby infer the chemical environment of the distal pocket, various isotopes, including  $^{13}\text{C}^{14}\text{N}$ ,  $^{12}\text{C}^{15}\text{N}$ ,  $^{13}\text{C}^{15}\text{N}$ , and  $^{12}\text{C}^{14}\text{N}$ , were used. In the low frequency region of the isotope difference spectra, at least two major isotope-sensitive bands were detected (Fig. 5A). We assigned the bands at 450 and 410  $\text{cm}^{-1}$  to the Fe– $\text{CN}^-$  stretching ( $\nu_{\text{Fe}-\text{CN}^-}$ ) and bending mode ( $\delta_{\text{Fe}-\text{CN}^-}$ ), respectively, associated with a linear but slightly tilted conformation of the  $\text{CN}^-$  ligand (27, 28). The assignment of the stretch and bend is supported by their respective disappearance in the  $\text{C}^{15}\text{N}-^{13}\text{CN}$  and  $^{13}\text{CN}-^{13}\text{C}^{15}\text{N}$  difference spectra (Fig. 5A). We also noted another, weaker bending mode at 440  $\text{cm}^{-1}$  that was assigned to a bent Fe–C–N conformation (27, 28). In the presence of L-Trp, similar stretching and bending modes were seen at 455 and 410  $\text{cm}^{-1}$ , respectively (Fig. 5B); the bending mode corresponding to a bent Fe–C–N linkage appeared at 444  $\text{cm}^{-1}$ . The enhancement of this mode in the presence of L-Trp suggests a steric and/or H-bonding interaction between the ligand and L-Trp. The other low frequency bands, which were not canceled out in the isotope difference spectra, are likely porphyrin modes coupled to the motion of the  $\text{CN}^-$  ligand (28).

**CO-bound Complex**—The high frequency region of the spectrum of the  $\text{Fe}^{2+}$ -CO complex of hIDO (Fig. 6B, top) indicated a six-coordinate and low spin complex. Addition of L-Trp caused similar changes to vinyl-associated bands as described above for the  $\text{Fe}^{3+}$ - $\text{CN}^-$  complex (Fig. 6B, bottom). The Fe–CO stretching ( $\nu_{\text{Fe}-\text{CO}}$ ) and bending ( $\delta_{\text{Fe}-\text{CO}}$ ) modes appeared prominently (Fig. 6A) at 518 and 577  $\text{cm}^{-1}$ , respectively. This assignment is supported by the appearance of two isotope-sensitive bands at 518 and 577  $\text{cm}^{-1}$  in the  $\text{CO}-^{13}\text{C}^{18}\text{O}$  difference spectrum (Fig. 7A, top).

In the presence of L-Trp,  $\nu_{\text{Fe}-\text{CO}}$  and  $\delta_{\text{Fe}-\text{CO}}$  shifted to 542 and 589  $\text{cm}^{-1}$  (Fig. 6A, bottom), respectively, as reflected by the associated strong bands in the  $\text{CO}-^{13}\text{C}^{18}\text{O}$  difference spectrum (Fig. 7A, bottom). The presence of L-Trp also caused the  $\delta_{\text{Fe}-\text{CO}}$  mode to be narrowed and intensified (Fig. 6A), indicating a steric and/or H-bonding interaction imposed by L-Trp to the Fe–C–O moiety. The internal C–O stretch  $\nu_{\text{C}-\text{O}}$  can sometimes be seen around 1900–1950  $\text{cm}^{-1}$  for CO-heme complexes. In the case of hIDO,  $\nu_{\text{C}-\text{O}}$  was not observed in the absence of L-Trp

TABLE I  
Iron-ligand vibrational frequencies ( $\text{cm}^{-1}$ ) for *hIDO* and other heme proteins

HRP, horseradish peroxidase; CCP, cytochrome-*c* peroxidase; ND, not determined; HS, high spin; LS, low spin.

Species	$\text{Fe}^{2+}$				$\text{Fe}^{3+}$		
	$\nu_{\text{Fe-His}}$	$\nu_{\text{Fe-CO}}$	$\delta_{\text{Fe-CO}}$	$\nu_{\text{C-O}}$	$\nu_{\text{Fe-CN}^-}$	$\delta_{\text{Fe-CN}^-}$	$\nu_{\text{Fe-OH}^-}$
<i>hIDO</i> -Trp	236	518	577	1933, 1953 <sup>a</sup>	450	410, 440	ND
<i>hIDO</i> +Trp	236	542	589	1901	455	410, 444	496, 546
Mb <sup>b</sup>	220	512	577	1944	453	ND	491 (HS) 550 (LS)
Hb <sup>c</sup>	215	507	578	1951	452	ND	492 (HS) 553 (LS)
HRP <sup>d</sup>	241, 244	531, 541	590	1906, 1933	453	405, 422	492 (HS) 502 (LS)
CCP <sup>e</sup>	227, 248	505, 537	587	1922, 1948	445	407, 445	ND

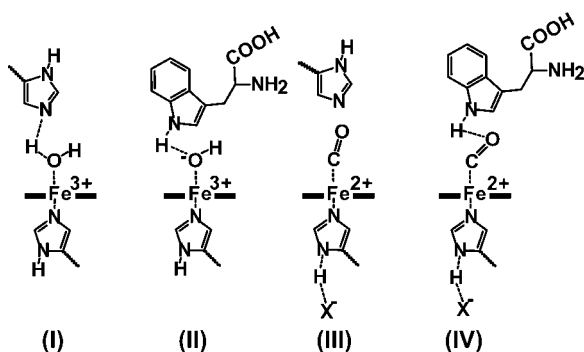
<sup>a</sup> Ref. 29.

<sup>b</sup> Refs. 22, 23, 28, 30, and 40.

<sup>c</sup> Refs. 22, 28, and 40.

<sup>d</sup> Refs. 27, 40, and 41.

<sup>e</sup> Refs. 27 and 40.



SCHEME 2. **Cartoon of the *hIDO* heme pocket.** The proposed heme pocket of *hIDO* is shown. The proximal and distal His residues are depicted with the latter engaged in H-bonding with distal water (I). Binding of Trp to the  $\text{Fe}^{3+}$  enzyme promotes distal hydroxide binding by stabilization through H-bonding (II). The  $\text{Fe}^{2+}$ -CO (III) and  $\text{Fe}^{2+}$ -CO-Trp (IV) complexes are also depicted. The analogous  $\text{CN}^-$  complexes would look similar to that depicted for CO. For the  $\text{Fe}^{2+}$  species, the proximal His is engaged in H-bonding with a neighboring amino acid residue ( $\text{X}^-$ ), which gives the imidazole ring of His imidazolate character that strengthens the proximal Fe-His bond.

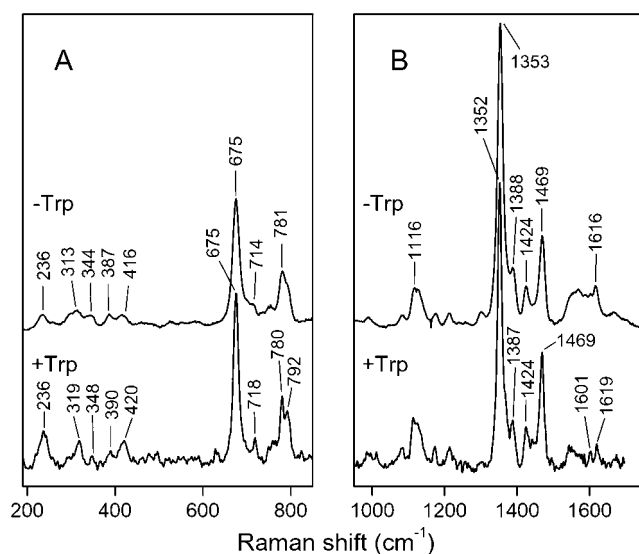


FIG. 3. **Resonance Raman spectra of ferrous *hIDO* in the absence and presence of L-Trp.** Experimental conditions were as described in Fig. 1 legend. Ferrous *hIDO* was prepared by mild dithionite reduction as described under "Experimental Procedures," and the final concentration of L-Trp in the bottom spectrum was 25 mM. For comparison, the intensity scale in panel A is half the scale in panel B.

(Fig. 7B, top). However, in the presence of L-Trp,  $\nu_{\text{C-O}}$  appeared at  $1901 \text{ cm}^{-1}$  (Fig. 7B, bottom), a value close to that determined by IR spectroscopy for *rIDO* (29).

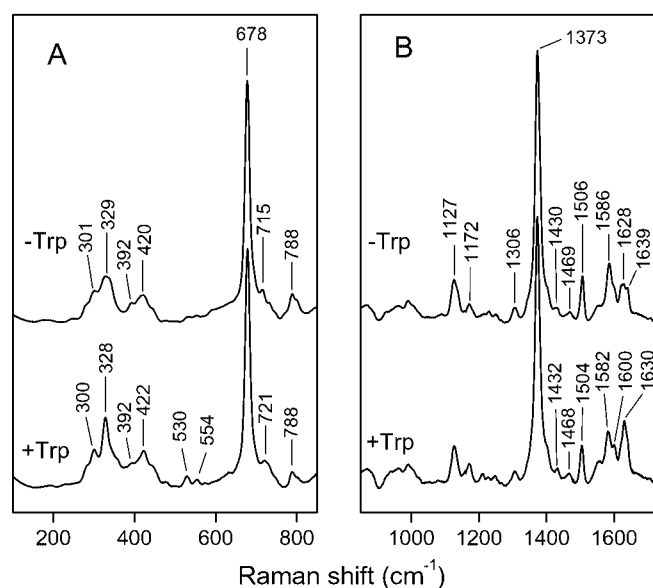


FIG. 4. **Resonance Raman spectra of the  $\text{Fe}^{3+}$ - $\text{CN}^-$  complex of *hIDO* in the absence and presence of L-Trp.** Panel A, low frequency region. Panel B, high frequency region. Experimental conditions were as described in Fig. 1 caption and the final concentration of L-Trp in the bottom spectrum was 5 mM.

Relating the frequencies of  $\nu_{\text{Fe-CO}}$  and  $\nu_{\text{C-O}}$  can give valuable information on the nature of the proximal ligand and the polarity of the distal pocket (see *e.g.* Refs. 25 and 30). Thus, separate correlation curves can be discerned for five-coordinate complexes and six-coordinate complexes with imidazole *versus* thiolate as proximal ligand (Fig. 8). The position along a curve is determined by either steric interactions or a local electric field generated by polar interactions. Positive dipoles originating from H-bonding interactions typically generate low  $\nu_{\text{C-O}}$  and high  $\nu_{\text{Fe-CO}}$ , whereas negative dipoles do the opposite (30). For example, in sperm whale Mb, the frequencies of the  $\nu_{\text{Fe-CO}}$  and  $\nu_{\text{C-O}}$  bands are  $512$  and  $1944 \text{ cm}^{-1}$ , respectively (30). As the distal His is mutated to a nonpolar residue,  $\nu_{\text{Fe-CO}}$  becomes lower, and  $\nu_{\text{C-O}}$  becomes higher as shown in Fig. 8 (31). Similar effects are observed for peroxidases (30, 32). The distal pockets of peroxidases are typically more polar than that in Mb; the data points therefore fall on the upper left corner of the imidazole correlation curve.

Assuming that the *hIDO* data point falls on the correlation curve 2 (Fig. 8), the  $\nu_{\text{C-O}}$  for the substrate-free *hIDO* is predicted to be  $\sim 1930 \text{ cm}^{-1}$  based on the  $\nu_{\text{Fe-CO}}$  mode observed at  $518 \text{ cm}^{-1}$ . This predicted value corresponds closely with one of the two  $\nu_{\text{C-O}}$  bands at  $1933$  and  $1953 \text{ cm}^{-1}$  observed in *rIDO* with the intensity of the  $1933 \text{ cm}^{-1}$  band less than half that of the  $1953 \text{ cm}^{-1}$  band (29). The fact that only the weaker isomer

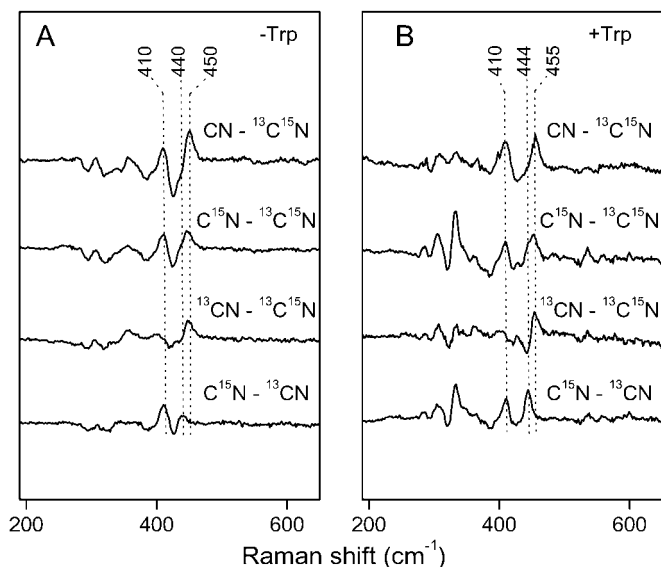


FIG. 5. Difference spectra for the  $\text{Fe}^{3+}\text{-CN}^-$  and  $\text{Fe}^{3+}\text{-CN}^-\text{-Trp}$  complexes in the low frequency region. The difference spectra were calculated for natural isotope  $\text{CN}^-$  complex minus the corresponding  $^{13}\text{C}^{15}\text{N}$ ,  $^{13}\text{CN}$ , and  $\text{C}^{15}\text{N}$  spectra in the absence (panel A) and presence (panel B) of L-Trp. The final concentration of L-Trp for the spectra in panel B was 5 mM.

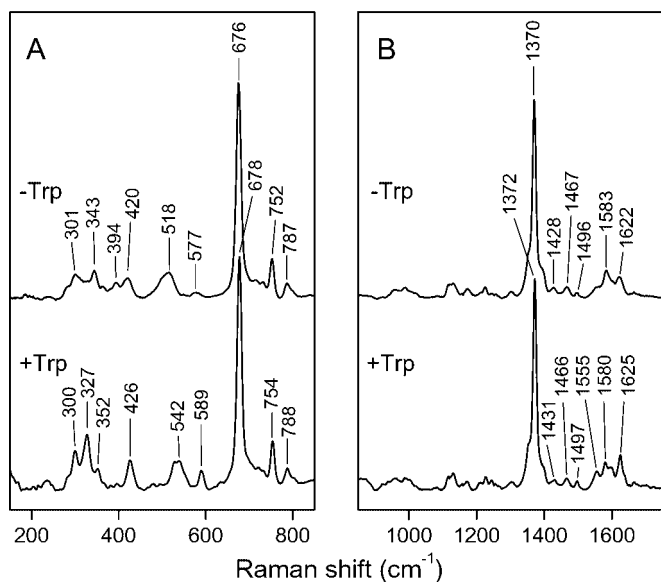


FIG. 6. Resonance Raman spectra of the  $\text{Fe}^{2+}\text{-CO}$  complex of hIDO in the absence and presence of L-Trp. Panel A, low frequency region. Panel B, high frequency region. Experimental conditions were as described in Fig. 1 legend except that the laser power used was <2 milliwatts to avoid photodissociation of the CO ligand. The final concentration of L-Trp in the bottom spectrum was 25 mM.

of rIDO was seen in hIDO suggests that the distal heme environment is slightly different in IDO from the two species. The position of the predicted hIDO data point in the correlation curve (Fig. 8) indicates further that the distal pocket of hIDO is slightly more polar than that in wild-type Mb although less polar than that in peroxidases. Binding of L-Trp caused the data point to shift to the upper left corner, corresponding to a more polar and peroxidase-like distal environment presumably due to the presence of a strong H-bond between L-Trp and CO.

#### DISCUSSION

The present resonance Raman characterization of the active site of hIDO revealed a blend of structural features common to

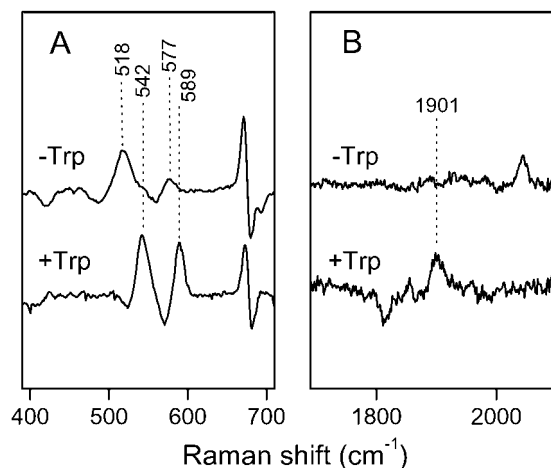


FIG. 7.  $\text{Fe}^{2+}\text{-CO-Fe}^{2+}\text{-}^{13}\text{C}^{18}\text{O}$  difference spectra for hIDO in the absence and presence of L-Trp. Panel A, low frequency region. Panel B, high frequency region. The final concentration of L-Trp in the bottom spectrum was 25 mM.

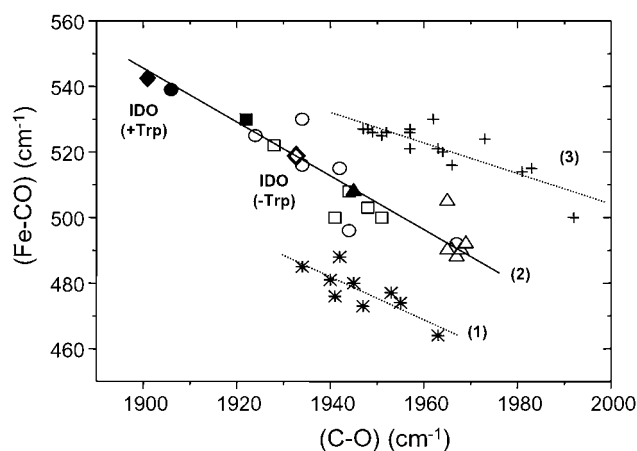
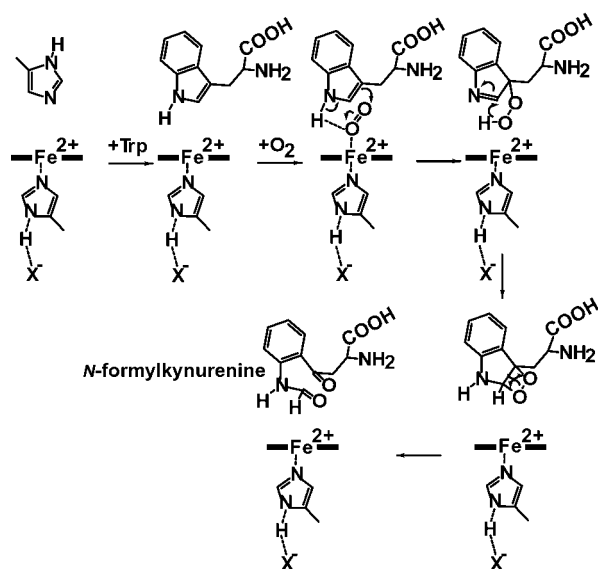


FIG. 8. Correlation of Fe-CO and C-O stretching frequencies for different heme proteins and porphyrin derivatives. Lines (1) and (2) are for complexes in which the proximal ligand is thiolate and histidine, respectively. Line (3) is for five-coordinate CO adducts. The open circles, open squares, and open triangles correspond to data obtained for horseradish peroxidase, cytochrome-c peroxidase, and myoglobin, respectively. The corresponding filled symbols represent data obtained from the wild-type proteins. The open and closed diamonds correspond to hIDO in the absence and presence of L-Trp, respectively. This figure is adapted from Refs. 30–32.

globins and peroxidases. In the  $\text{Fe}^{3+}$  state hIDO is six-coordinate with a distal water/hydroxide ligand similar to globins, whereas the  $\text{Fe}^{2+}$  species displays a peroxidase-like proximal Fe-His bond. The polarity of the distal pocket of hIDO is intermediate between that of globins and peroxidases. Binding of L-Trp reconditions the distal pocket to a peroxidase-like and sterically congested polar environment, which imposes strong steric and/or H-bonding interactions to the heme-bound ligands, although the proximal Fe-His bond strength is not affected. The strong proximal Fe-His bond and the unique distal environment provided by L-Trp likely play a crucial role in the enzymatic activity of hIDO.

**Proximal Heme Environment**—The present study on hIDO and previous spectroscopic work limited to rIDO (17) establish His as the proximal (fifth) ligand. This is indicated *e.g.* by  $\nu_4$  at  $1353\text{ cm}^{-1}$  in  $\text{Fe}^{2+}$  hIDO (Fig. 3B) and the  $\nu_{\text{Fe-CO}}/\nu_{\text{C-O}}$  data points falling on the His correlation curve (Fig. 8). Two highly conserved His residues have been identified in mammalian IDO and the IDO-like Mb of archaeogastropods (7) that correspond to His<sup>346</sup> and His<sup>303</sup> in hIDO (33). Replacement of His<sup>346</sup>



SCHEME 3. Schematic of the IDO-catalyzed oxidation of Trp. See text for details. The NH group of the proximal His is H-bonded to a neighboring amino acid residue ( $X^-$ ) as indicated by a weakened N–H bond of the proximal His represented by the dash lines.

with Ala by site-directed mutation prevents heme binding and decreases dioxygenase activity, whereas replacement of His<sup>303</sup> with Ala has no effect on heme content or activity,<sup>2</sup> suggesting strongly that His<sup>346</sup> is the proximal ligand for hIDO.

The Fe<sup>2+</sup> hIDO spectrum displayed a  $\nu_{\text{Fe-His}}$  band at 236  $\text{cm}^{-1}$  (Fig. 3), suggestive of a relatively strong Fe–His bond similar to that seen in peroxidases. The latter has been linked to an H-bond between the NH group of proximal His and the carboxylate group of a nearby Asp residue (26), giving the His an imidazolite character that strengthens the Fe–His bond. In some cases, such as dehaloperoxidase, the peptide C=O group of a proximal residue can also interact with the proximal His to produce a strong Fe–His bond (34). Our data therefore suggest that the proximal His residue in Fe<sup>2+</sup> hIDO may similarly be engaged in H-bonding with a presently undetermined, neighboring amino acid residue (indicated by  $X^-$  in Schemes 2 and 3).

**Distal Heme Environment**—The distal binding site in most ferric mammalian globins is occupied by a water molecule at neutral pH, and as a result, the electronic configuration of the heme iron is normally a six-coordinate high spin and low spin mixture. On the other hand, the strong proximal Fe–His bond in peroxidases, such as cytochrome-*c* peroxidase, forces the iron to move out of the porphyrin plane and thereby prevents the coordination of a weak distal water ligand to the heme. The ferric protein in most peroxidases thus favors a five-coordinate structure (35). The six-coordinate configuration of the Fe<sup>3+</sup> hIDO therefore suggests that the proximal Fe–His bond is not as strong as in the Fe<sup>2+</sup> hIDO. This may be due to differences in protein conformation between Fe<sup>3+</sup> and Fe<sup>2+</sup> hIDO similar to those reported for rIDO based on CD spectroscopic studies (17). A weaker Fe–His bond would be expected for Fe<sup>3+</sup> hIDO if its conformation disfavors the H-bonding interaction between the proximal His ligand and the neighboring residue  $X^-$ .

Like mammalian globins, the Fe<sup>3+</sup> hIDO is predominantly high spin at neutral pH, and the weak low spin signal increased at alkaline pH (data not shown), suggesting that the weak field ligand water is partially replaced by a strong field ligand OH<sup>-</sup> due to deprotonation. It is plausible that the heme-bound water is stabilized by the distal His<sup>303</sup> through H-bonding as illus-

trated in Scheme 2I based on amino acid alignment and spectroscopic evidence reported by others (6). The six-coordinate mixed spin character of IDO was also observed in Fe<sup>3+</sup> rIDO using EPR spectroscopy (17). However, in that study, Sono (17) suggested the a His residue, instead of a water molecule, is the sixth ligand coordinated to the heme iron. Histidine is a strong field heme ligand, which is typically associated with a low spin configuration. The mixed spin character of rIDO was thus attributed to a sterically hindered His (17). Based on the present data, we consider water to be a more likely distal ligand in Fe<sup>3+</sup> hIDO.

The binding of L-Trp in the distal pocket introduces significant conformational changes to the heme peripheral groups as suggested by the changes in the vibrational modes associated with the vinyl groups. The L-Trp also modified the chemical environment of the distal pocket as reflected by the pronounced transition from a six-coordinate mixed spin configuration to a low spin configuration (Fig. 1B) and the appearance of the two  $\nu_{\text{Fe-OH}^-}$  modes in the Raman spectrum, which are attributed to the H-bonding interaction between the OH<sup>-</sup> ligand and the NH group of the pyrrole ring of the L-Trp (Scheme 2II).

In the absence of L-Trp, the putative distal His<sup>303</sup> may also impose a steric influence and/or H-bonding interaction on other exogenous distal ligands such as CN<sup>-</sup> and CO for the ferric and ferrous protein, respectively. This is supported by the presence of a bent conformation for the Fe–CN<sup>-</sup> complex and the position of the data point for the Fe–CO complex on the  $\nu_{\text{Fe-CO}}$  versus  $\nu_{\text{C-O}}$  correlation plot (Fig. 8). The latter suggests that the distal environment of hIDO is slightly more polar than that in Mb and less polar than that in peroxidases. Binding of L-Trp caused the  $\nu_{\text{Fe-CO}}$ / $\nu_{\text{C-O}}$  data point to shift to the upper left end of the correlation curve in Fig. 8, indicative of strong H-bonding between L-Trp and CO (Scheme 2IV). The frequency and intensity of  $\delta_{\text{Fe-CO}}$  also increased markedly in the presence of L-Trp as predicted for a greater steric distortion of the Fe–C–O moiety. Similarly in the ferric protein, the intensity of the bending mode associated with a bent Fe–C–N form was increased by L-Trp, and the frequency of the stretch  $\nu_{\text{Fe-CN}^-}$  was 5  $\text{cm}^{-1}$  higher in the presence than in the absence of L-Trp (Table I). Together these data indicate that the substrate is placed in very close proximity to the distal ligands, which allows for mutual H-bonding and causes some steric distortion of the ligand coordination geometry. We suggest that such an interaction between L-Trp (or other substrates) and O<sub>2</sub> is one of the principal driving forces for the reaction catalyzed by IDO (see below). The fact that His<sup>303</sup> appears to have no catalytic significance according to mutation studies (see above) suggests that in the catalytic reaction L-Trp occupies and overwhelmingly determines the distal heme pocket environment experienced by a distal ligand as concluded from our data.

**Substrate-Heme Interactions**—Throughout this work we noted binding of L-Trp in the distal pocket substantially affects the conformation of the heme vinyl groups. Ferric hIDO displayed a single vinyl stretching band at 1621  $\text{cm}^{-1}$ , indicating similar orientation (relative to the heme plane) for both heme vinyl groups (35). Upon binding of L-Trp, the frequency of the stretching band increased, suggesting that the binding of the substrate forces the vinyl groups further out of the heme plane. This effect is independent of the spin and coordination state of the heme iron (e.g. Figs. 3, 4, and 6), suggesting that they were due to either direct interaction between L-Trp and the vinyl group(s) or due to L-Trp-induced protein conformational changes that modulate the conformation of the vinyl groups through direct contact between the vinyl groups and the surrounding protein matrix. L-Trp-induced protein conformational changes have been proposed for rIDO (17). The functional

<sup>2</sup> T. K. Littlejohn and R. J. W. Truscott, unpublished data.

significance of the substrate-driven conformational changes is unclear; however, we speculate that such changes are required to suitably orient the substrate in the distal pocket, *e.g.* for H-bonding with the heme-bound diatomic ligand as illustrated in Scheme 2. In Scheme 2, the indole ring of L-Trp is positioned perpendicular to the heme plane for simplicity, although a parallel orientation may be possible.

**Implications for Catalytic Reaction**—We showed that Fe<sup>2+</sup> hIDO has a very strong proximal Fe–His bond like peroxidases. Binding of L-Trp in the distal pocket does not affect the Fe–His bond strength; however, it reconditions the distal pocket to a more polar and sterically congested chemical environment. In peroxidases, the cleavage of the peroxide O–O bond is facilitated by a combination of the strong proximal Fe–His bond and the polar distal environment providing necessary H-bonding interactions based on the “push-pull” mechanism (36). The reaction catalyzed by IDO is inherently different from that of peroxidases. Whereas peroxidases carry out a heme iron-catalyzed cleavage of the O–O bond, IDO catalyzes the electrophilic addition of O<sub>2</sub> into the pyrrole ring of L-Trp, leading to the likely formation of a 3-hydroperoxyindolenine intermediate (37). The O–O bond breakage occurs later, which may not require the catalysis by the heme iron. Despite the differences in the overall nature of the catalytic mechanisms, the similarity in the heme pockets of IDO and peroxidases suggest that hIDO utilizes similar mechanisms to modulate the chemical properties of dioxygen.

Scheme 3 outlines a possible catalytic reaction mechanism. Accordingly the catalytically active Fe<sup>2+</sup> IDO is five-coordinate with the distal heme iron coordination position open for binding of substrates. L-Trp binds first in close proximity (but not directly) to the distal heme iron coordination position. It is followed by the binding of dioxygen to the sixth coordination position of the heme iron. The heme-bound dioxygen interacts with L-Trp through an H-bond between its proximal oxygen atom and the NH group of the pyrrole ring of L-Trp. The electronic effect imposed by this H-bond and the imidazolite character of the strong proximal Fe–His bond facilitates the electrophilic addition of the dioxygen to the pyrrole ring. We note that *N*-methyl-Trp and the thiophene and furan analogs (in which the pyrrole nitrogen atom is replaced by a sulfur or oxygen atom, respectively), which cannot form an H-bond, bind to but are not catabolized by IDO (16). Also, addition of electron-donating groups (*e.g.* methyl) at the *five* or *six* position of L-Trp enhances the reactivity of the substrate, whereas electron-withdrawing groups (*e.g.* -NO<sub>2</sub>) have the opposite effect (38). Together these data strongly suggest an electrophilic reaction that involves O<sub>2</sub> attacking the double bond between C-2 and C-3 in indole (Scheme 3). The resulting 3-hydroperoxyindolenine is strongly implicated as intermediate from previous chemical studies (37). We speculate, based on known, nonenzymatic oxidative chemistry of Trp (39), that the primary product of the catalytic reaction of IDO, *N*-formylkynurenine, is then formed via an endoperoxide intermediate. Further studies are required to establish the mechanism outlined in Scheme 3,

although the present study highlights the importance of and specific manner in which hIDO arranges the substrate for reaction with O<sub>2</sub> in the heme pocket.

**Acknowledgments**—We thank Dr. Bradley Collins and Sushila Thomas for experimental assistance and Drs. Denis Rousseau and Peter Southwell-Keely for helpful discussions.

## REFERENCES

- Hayaishi, O. (1985) *Biken J.* **28**, 39–49
- Yoshida, R., and Hayaishi, O. (1987) *Methods Enzymol.* **142**, 188–195
- Thomas, S. R., and Stocker, R. (1999) *Redox Rep.* **4**, 199–220
- Hirata, F., Ohnishi, T., and Hayaishi, O. (1977) *J. Biol. Chem.* **252**, 4637–4642
- Suzuki, T., and Takagi, T. (1992) *J. Mol. Biol.* **228**, 698–700
- Suzuki, T., Kawamichi, H., and Imai, K. (1998) *J. Protein Chem.* **17**, 817–826
- Suzuki, T., Kawamichi, H., and Imai, K. (1998) *Comp. Biochem. Physiol. B Biochem. Mol. Biol.* **121**, 117–128
- Ohnishi, T., Hirata, F., and Hayaishi, O. (1977) *J. Biol. Chem.* **252**, 4643–4647
- Hayaishi, O., Hirata, F., Ohnishi, T., Henry, J. P., Rosenthal, I., and Katoh, A. (1977) *J. Biol. Chem.* **252**, 3548–3550
- Taniguchi, T., Sono, M., Hirata, F., Hayaishi, O., Tamura, M., Hayasi, K., Izuka, T., and Ishimura, Y. (1979) *J. Biol. Chem.* **254**, 3288–3294
- Sono, M., Taniguchi, T., Watanabe, Y., and Hayaishi, O. (1980) *J. Biol. Chem.* **255**, 1339–1345
- Sono, M. (1989) *J. Biol. Chem.* **264**, 1616–1622
- Sono, M. (1989) *Biochemistry* **28**, 5400–5407
- Sono, M., and Cady, S. G. (1989) *Biochemistry* **28**, 5392–5399
- Sono, M. (1990) *Biochemistry* **29**, 1451–1460
- Cady, S. G., and Sono, M. (1991) *Arch. Biochem. Biophys.* **291**, 326–333
- Sono, M., and Dawson, J. H. (1984) *Biochim. Biophys. Acta* **789**, 170–187
- Littlejohn, T. K., Takikawa, O., Skylas, D., Jamie, J. F., Walker, M. J., and Truscott, R. J. W. (2000) *Protein Expr. Purif.* **19**, 22–29
- Yeh, S. R., Couture, M., Ouellet, Y., Guertin, M., and Rousseau, D. L. (2000) *J. Biol. Chem.* **275**, 1679–1684
- Spiro, T. G., and Li, X. Y. (1988) in *Biological Applications of Raman Spectroscopy* (Spiro, T. G., ed) pp. 1–37, John Wiley & Sons, New York
- Wang, J., Caughey, W. S., and Rousseau, D. L. (1996) in *Methods in Nitric Oxide Research* (Feelisch, M., and Stammler, J. S., eds) pp. 427–454, John Wiley & Sons, New York
- Feis, A., Marzocchi, M. P., Paoli, M., and Smulevich, G. (1994) *Biochemistry* **33**, 4577–4583
- Hu, S., Smith, K. M., and Spiro, T. G. (1996) *J. Am. Chem. Soc.* **118**, 12638–12646
- Li, X.-Y., Czernuszewicz, R. S., Kincaid, J. R., Stein, P., and Spiro, T. G. (1990) *J. Phys. Chem.* **94**, 47–61
- Yu, N. T., and Kerr, E. A. (1988) in *Biological Applications of Raman Spectroscopy* (Spiro, T. G., ed) pp. 39–95, John Wiley & Sons, New York
- Smulevich, G. (1993) *Biomolecular Spectroscopy, Part A* (Clark, R. J. H., and Hester, R. E., eds) pp. 163–193, John Wiley & Sons, New York
- al-Mustafa, J., Sykora, M., and Kincaid, J. R. (1995) *J. Biol. Chem.* **270**, 10449–10460
- Hirota, S., Ogura, T., Shinzawa-Itoh, K., Yoshikawa, S., and Kitagawa, T. (1996) *J. Phys. Chem.* **100**, 15274–15279
- Uchida, K., Bandow, H., Makino, R., Sakaguchi, K., Izuka, T., and Ishimura, Y. (1985) *J. Biol. Chem.* **260**, 1400–1406
- Vogel, K. M., Kozlowski, P. M., Zgierski, M. Z., and Spiro, T. G. (2000) *Inorg. Chim. Acta* **297**, 11–17
- Li, T., Quillin, M. L., Phillips, G. N., Jr., and Olson, J. S. (1994) *Biochemistry* **33**, 1433–1446
- Feis, A., Rodriguez-Lopez, J. N., Thorneley, R. N., and Smulevich, G. (1998) *Biochemistry* **37**, 13575–13581
- Tone, S., Takikawa, O., Habara-Ohkubo, A., Kadoya, A., Yoshida, R., and Kido, R. (1990) *Nucleic Acids Res.* **18**, 367
- Franzen, S., Roach, M. P., Chen, Y.-P., Dyer, R. B., Woodruff, W. H., and Dawson, J. H. (1998) *J. Am. Chem. Soc.* **120**, 4658–4661
- Smulevich, G. (1998) *Biospectroscopy* **4**, S3–17
- Dawson, J. H. (1988) *Science* **240**, 433–439
- Nakagawa, M., Watanabe, H., Kodato, S., Okajima, H., Hino, T., Flippen, J. L., and Witkop, B. (1977) *Proc. Natl. Acad. Sci. U. S. A.* **74**, 4730–4733
- Southan, M. D., Truscott, R. J. W., Jamie, J. F., Pelosi, L., Walker, M. J., Maeda, H., Iwamoto, Y., and Tone, S. (1996) *Med. Chem. Res.* **343**–352
- Witkop, B., and Patrick, J. B. (1951) *J. Am. Chem. Soc.* **73**, 2196–2200
- Dasgupta, S., Rousseau, D. L., Anni, H., and Yonetani, T. (1989) *J. Biol. Chem.* **264**, 654–662
- al-Mustafa, J., and Kincaid, J. R. (1994) *Biochemistry* **33**, 2191–2197